Frequency-Dependent Motor Model for Studying Interruption of Small Inductive Currents

R. S. Ferreira, M. V. M. S. Silva

***Abstract*— High-voltage vacuum switches have the characteristics of chopping the current before zero crossing and the capability to interrupt high-frequency currents, which can lead to the occurrence of voltage escalation in motor terminals due to the interruption of small inductive currents. Normally, in an industrial power system, the worst case of overvoltage in motor terminals happens during an aborted start, in which the locked rotor current must be interrupted by the vacuum switch, circuit breaker or contactor. The existing simulation models presented in the literature consider the motor as a constant impedance modeled by the locked rotor impedance at rated frequency, considering current amplitude and power factor. However, the high-frequency characteristic of the motor windings due to the overvoltage that appears during switch interruption is not considered, which can lead to very conservative results. In this paper, a frequency-dependent motor model for studying small inductive currents is presented and evaluated. The model can represent the locked rotor condition as well as the high-frequency behavior of motor windings. The proposed model is obtained from standardized tests to which high-voltage motors are normally subjected. The model was applied in an industrial power system with a wide range of power ratings and cable lengths.**

***Keywords*: frequency-dependent motor model, industrial power system, interruption of small inductive current, vacuum switch.**

I. Introduction

It is well known from the literature that the switching of vacuum devices can lead to high-overvoltages in motor and transformers terminals due to their ability to chopping the current before zero crossing and the capability to interrupt high-frequency currents [1]-[5].

In industrial power system, switching overvoltages may occur when vacuum circuit breakers or vacuum contactors are utilized, leading to switching transients known as multiple restrikes when the high-voltage motor is turned off. These transients are influenced by various installation and design factors, including, the arc-extinguishing principle of the switch; the size of the motor; the length of the power supply cable; system capacitance, among other factors [6].

In some cases, multiple restrikes can cause overvoltages that exceed the insulation capacity of the motor stator winding, resulting in insulation degradation and including sparks, which can be very critical in hazardous area applications. To mitigate this, surge protection should be installed at the motor terminals or another possibility is to specify stator windings with an enhanced insulation system which withstands higher voltage impulse levels [6][7].

Considering industrial power systems, the worst-case scenario of overvoltage at motor terminals is due to the interruption of small inductive currents in a locked rotor condition. In [6] it is indicated that overvoltage is more likely to occur when high-voltage motors with starting currents greater than 600 A are disconnected during startup or under stalled or overload conditions.

Even though voltage scalation due to vacuum switches is a well-known event in the literature, it lacks frequency dependent machine models to accurately predict the overvoltage at motor terminals. The existing simulation models available in the literature consider the motor as a constant impedance modeled by the locked rotor condition, taking into account starting current and power factor. However, the high-frequency characteristics of the motor windings are not considered, which can lead to very conservative results. Frequency-dependent models for high-voltage motors are generally very complex and are typically used to study voltage distribution within the motor windings [8][9]. These models usually require detailed geometrical information of rotating machines, making them highly intricate for system simulations.

In this paper, a simple frequency-dependent motor model for studying small inductive currents is presented and evaluated. The model is able to represent the locked rotor condition as well as the high-frequency behavior of motor windings. The high-proposed model is obtained from standardized tests to which high-voltage motors are normally subjected. The model was applied in an industrial power system with a wide range of power ratings for different cable lengths.

The following research contributions and novelties can be summarized:

- ✓ a simplified frequency-dependent motor model for studying the interruption of small inductive currents;
- ✓ the model is derived from standardized tests commonly applied to high-voltage motors;
- ✓ the proposed model was successfully applied in an industrial power system with various power ratings and cable lengths;
- ✓ the proposed model can be used to optimize the use of surge protection, as simpler models always require it;
- ✓ the proposed model can be easily expanded to develop transient models for other electromagnetic events in rotating machines.

R. S. Ferreira is with Petróleo Brasileiro S.A. - Petrobras, Rio de Janeiro, Brazil (e-mail of corresponding author: rodrigosousa@petrobras.com.br).
M. V. M. S. Silva is with Petróleo Brasileiro S.A. - Petrobras, Rio de Janeiro, Brazil (e-mail: matheus.venancio@petrobras.com.br).

Paper submitted to the International Conference on Power Systems Transients (IPST2025) in Guadalajara, Mexico, June 8-12, 2025.

II. MOTOR FREQUENCY-DEPENDENT MODEL

The worst-case scenario of overvoltage during the interruption of small inductive currents in induction motors occurs during an abnormal start, specifically when the motor attempts to start but the rotor remains locked. In this situation, the protection equipment (relays and circuit breaker or contactor) activate before the locked rotor time is reached. Consequently, the switch interrupts the motor's inductive starting current. Therefore, the motor model must accurately represent the locked rotor condition, including the current amplitude and power factor, before the switch begins to open to ensure the correct current is interrupted. Additionally, the model must capture the motor's high-frequency behavior to account for the overvoltage that appears at the motor terminals after the switch starts to open.

The proposed model to simulate an aborted starting uses the information of locked rotor current ratio and starting power factor to model the locked rotor impedance at rated frequency. In addition, the results of capacitance from tan delta test and Surge test, which are standard tests performed in high-voltage motors, are used to obtain the high-frequency impedance of the proposed model. The proposed model is depicted in Fig. 1 which is based on the n-branch model presented in [10], and it is obtained by using rated-frequency and high-frequency impedances.

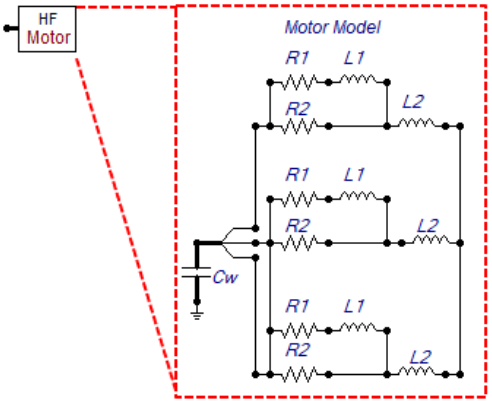

Fig. 1. Frequency-dependent motor model proposed.

The capacitance of the stator windings (C_w) obtained from tan delta test [11] is used in the model as shown in Fig. 1.

The resistances and inductances of the model (R_1, R_2, L_1 and L_2) are determined based on the values calculated for both locked rotor and high-frequency conditions. The locked rotor resistance and inductance are derived using the locked rotor current ratio and the starting power factor. The high-frequency impedance is obtained from the Surge test, as explained later. With these two sets of inductances and resistances, it is possible to create the two-branch model shown in Fig. 1. The resistances and inductances (R_1, R_2, L_1 and L_2) are calculated to ensure that the equivalent impedance for each frequency matches both the locked rotor and high-frequency conditions. Equations presented in [10] are used to calculate the parameters.

A. Surge test

Using the results of the Surge test for the complete stator windings [12] is possible to determine the motor high-frequency behaviour. The surge test procedure can be understood by the scheme depicted in Fig. 2. The capacitance of the surge tester (C_S) is charged from zero up to the voltage test, and when the required voltage is achieved, the switch (S) is closed, and the capacitor discharge in the motor's winding.

The result is a damped oscillatory waveform which frequency depends on the stator windings high-frequency parameters (capacitance, inductance, and resistance).

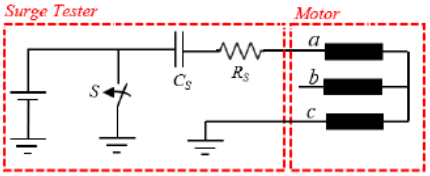

Fig. 2. Surge test scheme for complete windings.

Therefore, by knowing the capacitance of the windings from the tan delta test, it is possible to determine the high-frequency resistance and inductance of the motor. Firstly, since the frequency of the oscillatory waveform is a result from the Surge test, the high-frequency inductance can be calculated using the known-capacitance and the Equation (1):

$$f = \frac{1}{2\pi\sqrt{L \cdot C}} \tag{1}$$

To obtain the high-frequency resistance, the damping of the oscillatory waveform from the Surge test results is used. In an RCL circuit, the time constant of the decay can be calculated using the Equation (2). As the inductance is already known the high-frequency resistance can be easily calculated:

$$\tau = \frac{2L}{R} \tag{2}$$

Fig. 3 summarizes a typical result from the Surge test and the methodology used to extract the high-voltage inductance and resistance.

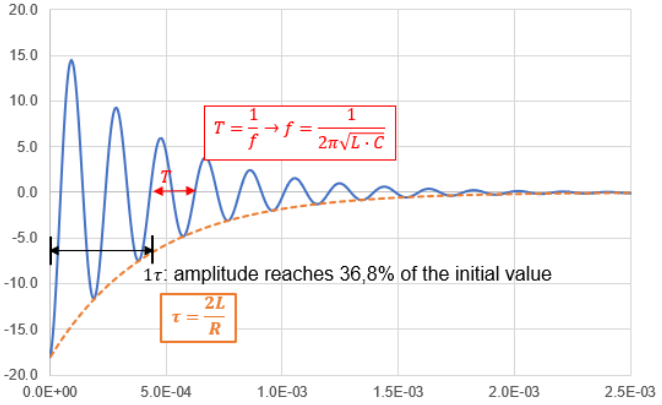

Fig. 3. High frequency impedance calculation.

B. Model Validation

In order to validate the model at rated and high-frequencies, different analysis have been performed:

High-Frequency Condition

Firstly, the surge test result (high-frequency behavior), was reproduced using the equivalent model presented in Fig. 4. For this analysis, the capacitance of the surge tester is discharged on the motor model and the oscillatory damped response is simulated by using the circuit depicted in Fig. 4. Results obtained in simulation and in a real surge test are presented in Fig. 5, and as can be seen the results are very similar, especially for the first oscillations where the reignition tends to occur.

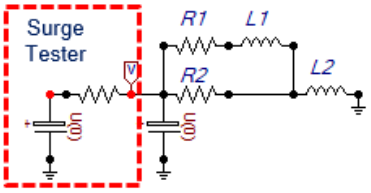

Fig. 4. High-frequency model validation.

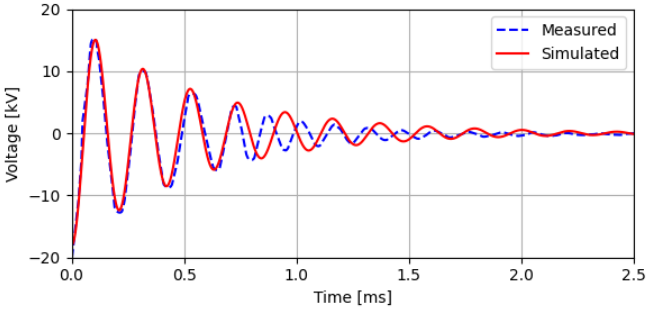

Fig. 5. Surge test result measured and simulated.

Locked rotor current interruption

It is important to verify that the frequency-dependent motor model can also accurately model the locked-rotor condition. Therefore, to better understand why the locked-rotor impedance model does not accurately represent the phenomenon, some evaluations using the simple circuits presented in Fig. 6, which represent a single phase of the three models for a 235 kW motor, are performed.

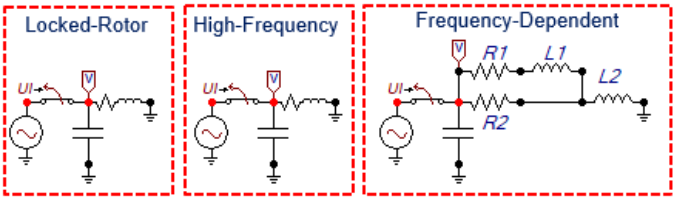

Fig. 6. Frequency-dependent model validation.

The models considered are:

- locked-rotor model: the motor is modelled by the locked rotor impedance, which is valid for rated frequency.
- high-frequency motor model: the motor is modelled by the high-frequency impedance, obtained from the surge test as explained previously;
- frequency-dependent model: the motor is modelled considering both conditions, locked rotor and high-frequency impedances.

The three circuits are considered under steady-state condition until the switch is suddenly opened to simulate current interruption. To compare the models, three variables are crucial for analysis: the current, the transient recovery voltage (TRV) at the switch, and the voltage at the motor terminals.

Considering Fig. 7, which shows the current, it can be observed that the proposed model accurately captures the 60Hz impedance, providing the correct starting current and power factor, ensuring the interruption occurs at the correct instant. In contrast, the high-frequency impedance model fails to provide accurate starting data, resulting in significant differences in current amplitude and the chopping current moment.

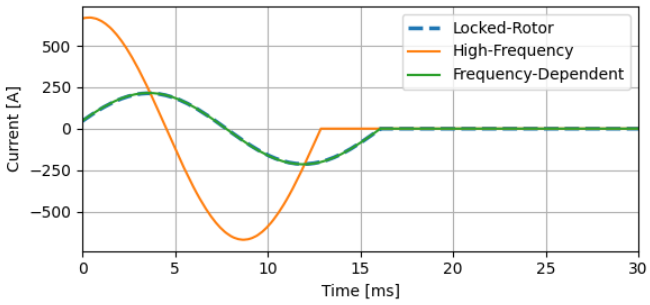

Fig. 7. Current for each model simulated.

Analyzing the TRV presented in Fig. 8 and Fig. 9, it is evident that the occurrence instant is the same for both the locked-rotor and frequency-dependent models, as they correctly model the starting current. However, the TRV behavior differs significantly between these two models in terms of oscillating frequency and damping. When the current reaches the chopping value, the voltage at the motor side oscillates based on its damped natural frequency. This behavior is accurately captured only by the high-frequency and frequency-dependent models, reflecting the true dynamics of the motor windings after the switch is opened.

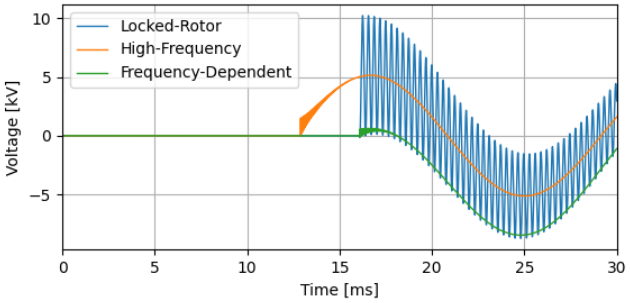

Fig. 8. TRV for each model simulated.

Therefore, as shown in Fig. 10, the voltage at the motor terminals is a combination of the locked-rotor and high-frequency models for each moment, before and after the current chopping. This behavior is accurately captured only by the proposed model.

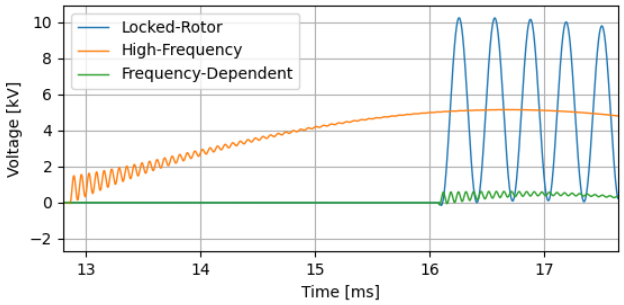

Fig. 9. TRV for each model simulated (zoomed in).

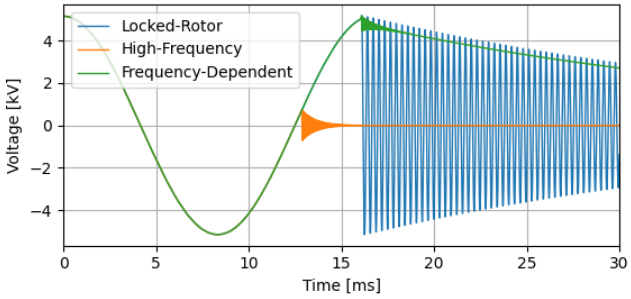

Fig. 10. Voltage at motor terminals for models compared.

Based on the previous results the proposed model is considered suitable for studying interruption of small inductive currents. The aforementioned methodology has been applied for different motor sizes, and TABLE I summarizes the parameters for all motor that will be analyzed in this paper.

TABLE I
HIGH-FREQUENCY MOTOR MODEL PARAMETERS.

Motor data		High-Frequency Motor Model				
[kV]	[kW]	R_1 [Ω]	R_2 [Ω]	L_1 [mH]	L_2 [mH]	C_W [μF]
13.8	14000	0.35	20.7	0.9	6.8	0.106
13.8	1250	0.80	49.0	46.3	38.9	0.041
6.3	1195	0.81	43.6	1.5	10.8	0.045
6.3	810	-0.67	14.3	12.1	5.7	0.071
6.3	550	-2.84	13.0	19.1	5.6	0.051
6.3	500	-4.84	7.7	12.6	3.8	0.037
6.3	450	-1.97	22.0	25.6	6.2	0.039
6.3	385	-6.04	10.1	17.8	5.0	0.041
6.3	300	-4.16	18.9	27.7	5.3	0.035
6.3	235	-7.32	7.6	6.8	2.8	0.037
6.3	185	-8.75	9.1	7.8	2.7	0.024

In some cases, negative values have been found for the resistance R_1. This is only a numerical value and does not pose a problem for the simulations, as the equivalent resistance for each frequency will always be positive as indicated in [10]. The equivalent resistance and inductance as a function of frequency for some of the motors, which have exhibited negative resistance R_1, is presented in Fig. 10. As shown in the figure, the equivalent resistance for all the motors remains positive across the entire frequency range of interest, ensuring the validity and accuracy of the results

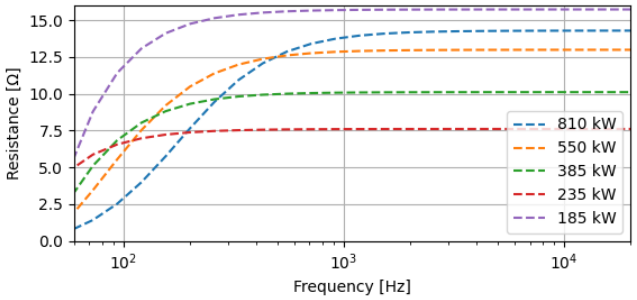

Fig. 11. Equivalent resistance for some of the motors simulated.

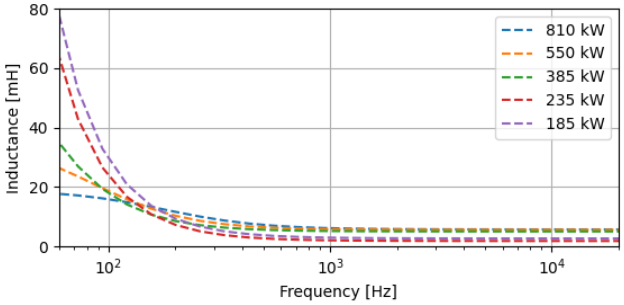

Fig. 12. Equivalent inductance for some of the motors simulated.

III. SYSTEM MODEL

The electrical system considered in the analysis has synchronous generators connected at the main 13.8 kV switchgear. The motors analyzed are connected directly to the 13.8 kV or at the 6.6 kV system by a step-down transformer as shown in Fig. 13. The worst results are obtained when there are no other loads in parallel to the motor which is being started, Therefore, the scheme presented at Fig. 13, without other loads, is used for system modelling during a motor starting at 6.6 kV system. In case the 13.8 kV motors are starting, the step-down transformer and the 6.6 kV system are out of operation. Details of each component model are presented in sequence.

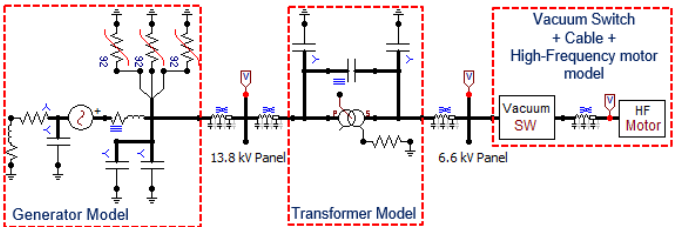

Fig. 13. Power system considered in the simulations.

A. Vacuum Switch

To study interruption of small inductive currents, the model of the switch, circuit breaker for bigger motors and contactor for smaller motors, has been implemented considering the following features based on [1][5]:

Chopping current (Ich)

The chopping current is the capability of the vacuum switches to interrupt the current before zero crossing.

Dielectric strength of the Cold gap

The dielectric strength capability of the cold gap (V_{sup}) of the vacuum switches depends on the distance of the contacts, which is modelled as per the following equation:

$$V_{sup} = A(t - t_{open}) + B \text{ [kV]} \quad (3)$$

where:

A is the rate of rise of the dielectric strength;

B: is the initial dielectric strength (supportability at the moment the contacts start to separate);

t_{open}: is the instant of time the contacts start to separate;

t: is the simulation time.

Quenching capability

The quenching characteristic indicates the capability of the vacuum switch to interrupt a high-frequency current and, normally, it is linked to the rate of rise of the current (*di/dt*). The quenching capability is modelled by the following time dependent equation:

$$\frac{di_{sup}}{dt} = C(t - t_{open}) + D \text{ [A/ µs]} \quad (4)$$

where:

C is the rate of rise of the quenching capability;

D: is the initial quenching capability.

Total time of contacts separation

Another parameter considered in the model is the total time to separate the contacts (Δt_{open}), which is calculated considering the opening velocity and the travel distance of the contacts.

The values used in simulations have been obtained for circuit breakers and contactors based on typical values and manufactures information, which are summarized in TABLE II.

TABLE II
VACUUM SWITCH PARAMETERS.

Parameter	Circuit Breaker		Contactor
	17.5 kV	12 kV	12 kV
Ich [A]	5	2.3	1
A [kV/ms]	20	20	20
B [kV]	1	1	1
C [A/µs²]	1	1	1
D [A/µs]	250	250	250
Δt_{open} [s]	0.01	0.01	0.01

Summarizing, the switch model monitors the current and the voltage between its contacts (TRV). Once the current on the switch is less than the chopping value the switch interrupts the current and a TRV appears. If the TRV is greater than the cold dielectric strength, which is time dependent, the arc reignites and will be interrupted again in the next zero crossing if the rate of rise of the current is less than que quenching capability. This process of interruption and reignition will repeat until the TRV does not exceed the dielectric strength of the switch. The switch model has been implemented by using MODELS simulation language from ATP [13].

B. Power Transformers

Power transformers are modelled using saturable models from ATP [13]. The required data are the short-circuit impedance (resistance and inductance), magnetizing branch model and saturation curve. Typical values for capacitance from primary and secondary windings to ground and between windings have been considered in the model. The transformer is delta-wye connected with the neutral grounded by a resistance.

C. Power Supply

The power supply is modelled as an ideal voltage source behind the sub-transient impedance. The internal voltage is considered as 13.8 kV, since the generators are simulated at no load before motor starting. Surge capacitors and arrestors are also considered in the model to represent the existent surge protection in the real generators. Additionally, the generators are grounded by a high resistance at the secondary of a grounding transformer, which have been modelled by an inductive-resistive impedance.

D. Cables

For the cables, a distributed Clarke model has been used [13]. This model considers the travel wave phenomenon, which is present in high-frequency studies. For cable parameters, typical values have been considered based on electrical parameters provided in the manufacturer's catalogue.

A more detailed JMARTI frequency-dependent model for cables between the vacuum switch and the motor has been evaluated to be used, however some numerical issues have been observed, and they were not considered in the analysis. The best approach would be the ULM (Universal Line Model) now presented in ATPDraw [13], however, as the studies consider the motor at locked-rotor as an initial permanent condition, ULM model cannot be used, since there is no steady-state initialization in ATP [13]. Therefore, the simple distributed Clarke model has been considered as the most suitable for the evaluations performed in this paper, moreover, it leads to more conservative results.

IV. STUDY CASES

The proposed motor model is applied for 13.8 kV and 6.3 kV motors in the system presented in Fig. 13. Simulations have been performed in a wide range of motor rated power in order to verify its influence on the motor overvoltages. TABLE III presents the main information of each case simulated.

For all the cases it has been considered that the switch will open exactly before the chopping current crossing, which is the worst condition to start the reignition, as the dielectric strength of the cold gap will be minimal when the TRV begins to occur.

TABLE III
SIMULATION CASES.

Case	Motor data		Cable data		Switch Type
	[kV]	[kW]	Formation	Length [m]	
1	13.8	14000	1x3/C#95	350	Circuit Breaker
2	13.8	1250	1x3/C#95	76	
3	6.3	1195	1x3/C#70	239	
4	6.3	810	1x3/C#50	120	Contactor
5	6.3	550	1x3/C#50	90	
6	6.3	500	1x3/C#50	312	
7	6.3	450	1x3/C#50	179	
8	6.3	385	1x3/C#50	306	
9	6.3	300	1x3/C#50	180	
10	6.3	235	1x3/C#50	181	
11	6.3	185	1x3/C#50	202	

As an acceptance criterion, the simulated overvoltages between motor terminals and neutral are compared with those indicated in IEC 60034-15 for steep-fronted impulses [7]. The limits for each voltage level are presented in TABLE IV, as the simulated motors are specified to withstand these levels.

TABLE IV
OVERVOLTAGE WITHSTOOD BY MOTORS.

Motor Rated Voltage [kV]	Limits of Overvoltage	
	Peak [kV]	Front Time [µs]
13.8	39	0.2
6.3	18	0.2

To better understand the events involved, the following figures present the results obtained for Case 8 (235 kW motor with cable length of 180 m). Fig. 14 shows the voltage between motor terminals and neutral and as can be seen no reignition has occurred, since according to Fig. 15 and Fig. 16 the transient recovery voltage in the vacuum switch is less than the cold gap strength just after the opening begins.

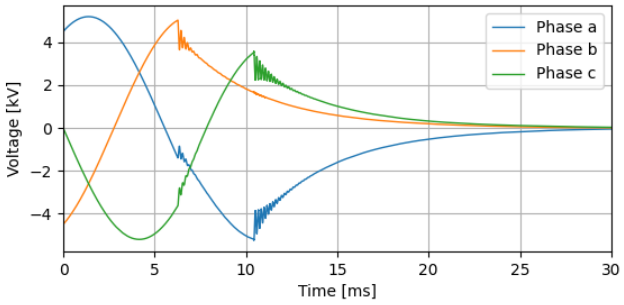

Fig. 14. Voltage between motor terminals and neutral for Case 8.

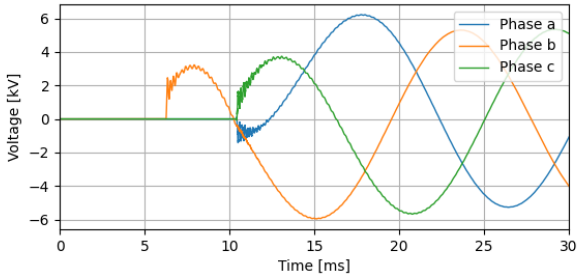

Fig. 15. TRV across the vacuum switch for Case 9.

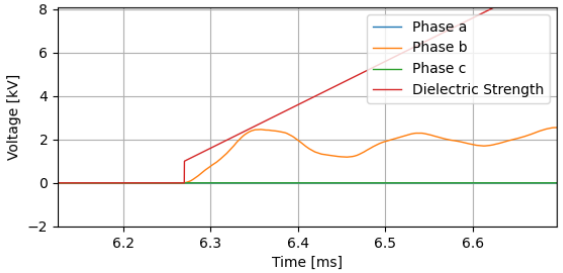

Fig. 16. TRV across the vacuum switch and dielectric strength of the cold gap for Case 9 (zoomed in).

In addition, Fig. 17 shows the expected current behavior. The starting current is at steady-state condition before the switch opens. The current is interrupted once it reaches the chopping value after the switch start to open.

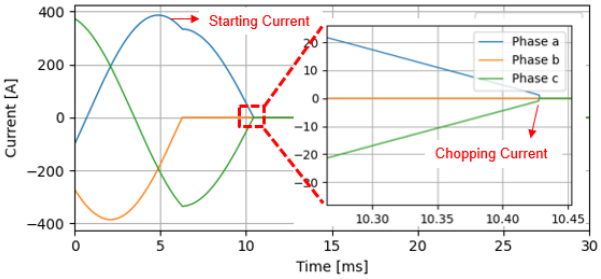

Fig. 17. Current in the switch for Case 9.

To compare with simpler motor models, Fig. 18 shows the overvoltage for Case 8 using a locked-rotor impedance model, which does not take high-frequency behavior into account. As can be seen the results by considering only the locked rotor impedance has presented conservative results, since the high-frequency transient recovery voltage, presented in Fig. 18 and Fig. 19, is not attenuated by the locked-rotor impedance model.

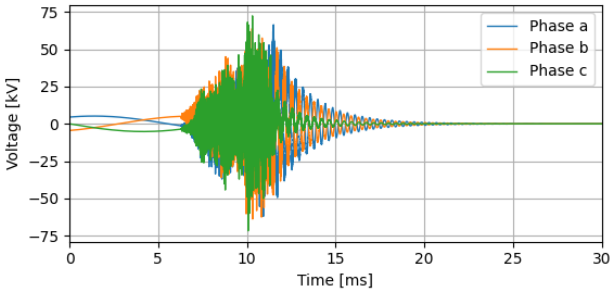

Fig. 18. Voltage between motor terminals and neutral for Case 9 using a locked-rotor impedance model.

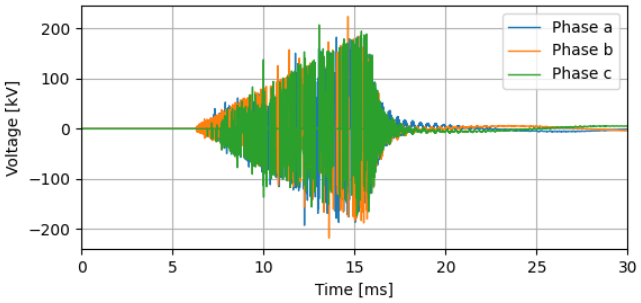

Fig. 19. TRV across the switch for Case 9 using a locked-rotor impedance model.

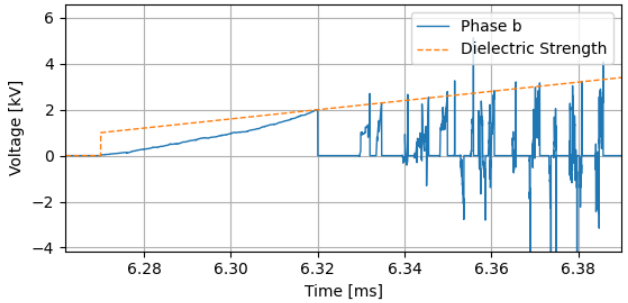

Fig. 20. TRV across the switch for Case 9 using a locked-rotor impedance model (zoomed in).

Fig. 21 and Fig. 22 show results where even with the frequency-dependent motor model the overvoltage found were above the acceptance criterion.

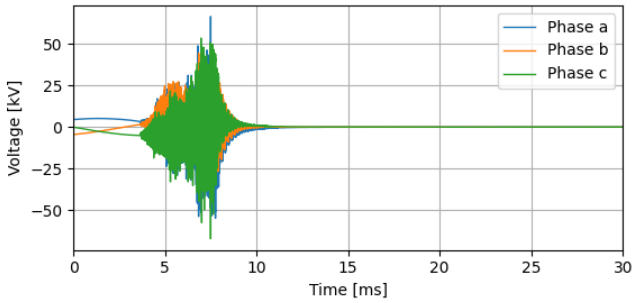

Fig. 21. Voltage between motor terminals and neutral for Case 7.

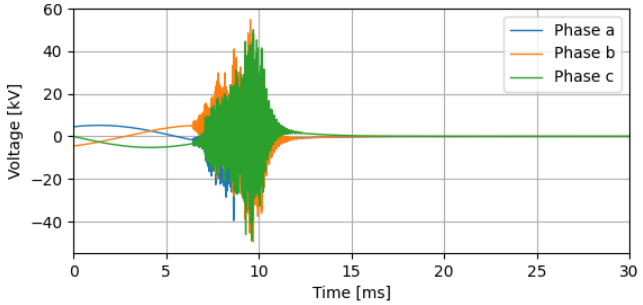

Fig. 22. Voltage between motor terminals and neutral for Case 9.

Considering the waveforms obtained for each case simulated, TABLE V summarizes the peak and front time of the overvoltages. Highlighted cells show when the acceptance criterion indicated in TABLE IV has been surpassed.

TABLE V
SIMULATION RESULTS.

Case	Simulation Results		
	Peak [kV]	Peak [pu]	Front Time [μs]]
1	161.4	14.3	74.0
2	86.8	7.7	1.0
3	118.4	23.0	2.0
4	43.4	8.4	2553
5	66.5	12.9	4.0
6	5.3	1.0	5015
7	67.1	13.0	6.2
8	5.2	1.0	4889
9	54.8	10.7	3.9
10	6.7	1.3	4972
11	6.7	1.3	5014

According to TABLE IV, in some cases the peak overvoltages have not surpassed the limits.

For 13.8 kV motors the peak values simulated are much greater than those which the motors are designed. However, in the 6.3 kV motors, the limits have not been surpassed for some motors, especially the smaller ones. For the biggest motors, the peak values were always surpassed. It is important to highlight that the time front is always much greater than the values which the motors are tested for both voltages studied, 13.8 kV and 6.3 kV.

In order to verify the influence of the cable other simulations have been performed for cables from 50 m to 500 m. Results are presented in TABLE VI only 6.3 kV motors, since the results for 13.8 kV motors are always above the limits for cable lengths up to 500 m.

TABLE VI
SIMULATION RESULTS AS A FUNCTION OF THE CABLE LENGTH.

Case	Motor data		Overvoltage [kV]					
	[kV]	[kW]	50 m	100 m	200 m	300 m	400m	500 m
3	6.3	1195	284.2	194.6	91.4	99.1	85.2	100.8
4	6.3	810	48.6	81.3	57.3	54.1	62.2	44.3
5	6.3	550	61.3	62.6	57.0	46.1	43.6	58.2
6	6.3	500	49.0	37.8	40.8	5.3	5.2	5.1
7	6.3	450	91.4	54.0	57.9	54.8	49.4	5.2
8	6.3	385	44.6	36.1	37.0	5.2	5.2	5.2
9	6.3	300	58.3	49.5	48.0	5.2	5.2	5.2
10	6.3	235	6.7	6.7	6.6	6.6	6.6	6.6
11	6.3	185	6.8	6.8	6.7	6.6	6.7	6.6

According to the data showed in TABLE VI it is possible to see that, in general, for longer cables the overvoltages are lower. In fact, for cables from 300 m most of the motors did not present results above the limits and for 500 m, all motors up to 500 kW have not presented overvoltages above the criterion.

Fig. 23 and Fig. 24 show the transient recovery voltage

(TRV) for Case 11, without the cable and with a 100 m cable length. As can be seen, the cable model, due to its distributed nature, attenuates the voltage, resulting in lower amplitude and frequency of the TRV compared to when the cable is disregarded. If a frequency-dependent cable model is used, these reductions tend to be even greater, as the overvoltage will still more attenuated.

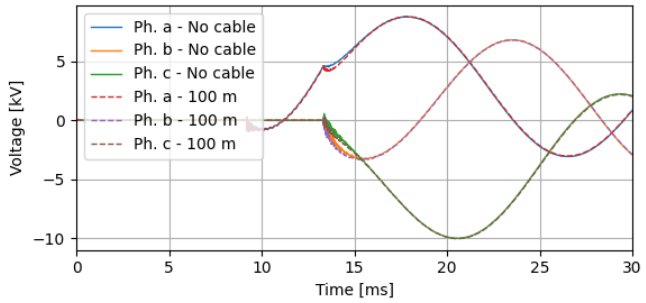

Fig. 23. TRV across the switch for Case 11 with no cable and 100 m of cable length.

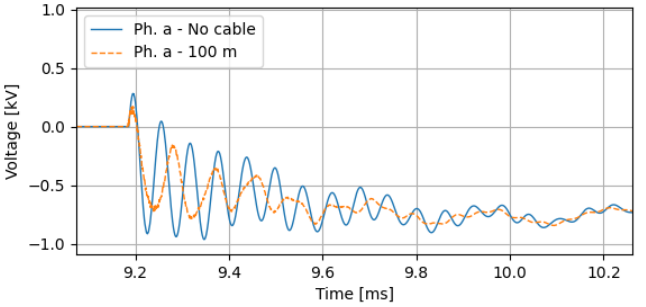

Fig. 24. TRV across the switch for Case 11 with no cable and 100 m of cable length. (zoomed in).

For motors that have shown results above their limits, surge protection is typically used. Apart from the results of this paper, surge protection is generally applied to all high-voltage motors above 6 kV, regardless of the motor's rated power and cable length. However, according to the results, some motors were not subjected to overvoltages higher than those for which they are designed, as per IEC 60034-15, especially for longer cables. The occurrence of overvoltage depends on the motor design, as well as cable and vacuum switch parameters. Nevertheless, since some of the smaller motors did not experience overvoltages above the limit, the results suggest that surge protection may not be necessary in these cases. Therefore, its use can be optimized when employing this more realistic motor model.

V. Conclusions

This paper presents and evaluates a frequency-dependent motor model designed to study interruption of small inductive currents. The model effectively considers both the locked rotor condition and the high-frequency behavior of motor windings. The high-frequency characteristics are derived from standardized tests typically conducted on high-voltage motors. The proposed model was applied to an industrial power system, encompassing a wide range of motor rated powers and supply cable lengths.

Regarding the 13.8 kV results, all simulated cases presented overvoltages above the criterion, indicating that additional protection is required for motor windings. For 6.3 kV motors, it was observed that reignitions occur at higher motor powers. According to the results, motors up to 500 kW did not exhibit overvoltages above the standard impulse levels for cable lengths of 500 m. For shorter cables, only the smallest motors did not present overvoltages. For powers equal to or greater than 500 kW, all motors experienced reignitions for all simulated cable lengths. Therefore, the results suggest that smaller motors may not require surge protection; however, the specific system, motor, and switch models should always be evaluated.

In summary, the main conclusion is that simulations with the frequency-dependent motor model result in lower overvoltages compared to simpler motor models that only consider locked rotor impedance. The use of this high-frequency model can optimize the utilization of surge protection, which is always required when simple models are used for the motor. Additionally, the proposed methodology can be easily expanded to develop transient models for other electromagnetic transient evaluations in rotating machine.

VI. References

[1] M. Popov, "Switching three-phase distribution transformers with a vacuum circuit breaker – analysis of overvoltage and protection of equipment", PhD dissertation, Delft University of Technology, 2002.

[2] D. D. Shipp, T. J. Dionise, V. Lorch, and W. G. MacFarlane, "Transformer failure due to circuit breaker induced switching transients," IEEE Trans. Ind. Appl., vol. 47, no. 2, pp. 707–718, Mar./Apr. 2011

[3] M. Popov and E. Acha, "Overvoltages due to switching off an unloaded transformer with a vacuum circuit breaker," in IEEE Transactions on Power Delivery, vol. 14, no. 4, pp. 1317-1326, Oct. 1999.

[4] J. Lopez-Roldan, H. de Herdt, T. Sels, D. van Dommelen, M. Popov, L. van der Sluis, and J. Declercq, "Analysis, simulation and testing of transformer insulation failures related to switching transients overvoltages," presented at the CIGRE, Paris, France, 2002, paper 12-116.

[5] D. Penkov, C. Vollet, B. De Metz-Noblat and R. Nikodem, "Overvoltage protection study on vacuum breaker switched MV motors," 2008 5th Petroleum and Chemical Industry Conference Europe - Electrical and Instrumentation Applications, Weimar, Germany, 2008, pp. 1-7.

[6] IEC 60079-14, Explosive atmospheres – Part 14: Electrical installations design, selection and erection, 2013.

[7] IEC 60034-15, Rotating electrical machines – Part 15: Impulse voltage withstand levels of form-wound stator coils for rotating a.c. machines, 2009.

[8] R.S. Ferreira, A.C. Ferreira, Transient model to study voltage distribution in electrical machine windings considering the rotor, Electric Power System Research Volume 195 (2021).

[9] R. S. Ferreira, A. C. Ferreira, Analysis of End-Windings Influence on the Transient Voltage Distribution in Machine Stator Windings by a Three Phase Model, in IEEE Transactions on Energy Conversion, vol. 36, no. 3, pp. 2110-2119 (2021).

[10] M. L. R. Chaves, J. C. Oliveira, J. W. Resende, A. M. Lopes, "Time Domain Cable Modeling with Frequency Dependent Parameters," IPST - International Power System Transients, Seattle, June 22-26, 2017.

[11] IEC 60037-27-3, Rotating electrical machines – Part 27-3: Dielectric dissipation factor measurement on stator winding insulation of rotating electrical machines, 2015.

[12] IEEE Std 522, IEEE Guide for Testing Turn Insulation of Form-Wound Stator Coils for Alternating-Current Electric Machines, 2023.

[13] H. K. Høidalen, L. Prikler, F. Peñaloza, ATPDRAW version 7.6 for Windows User's Manual, 2023.